Neuron, Vol. 21, 191–202, July, 1998, Copyright ©1998 by Cell Press

Cue-Invariant Activation in Object-Related Areas of the Human Occipital Lobe

Kalanit Grill-Spector,* Tamar Kushnir,† Shimon Edelman,‡ Yacov Itzchak,† and Rafael Malach*§
*Weizmann Institute of Science
Rehovot 76100
†Diagnostic Imaging Department
The Chaim Sheba Medical Center
Tel Hashomer 52621
Israel
‡School of Cognitive and Computing Sciences
University of Sussex, Falmer
Brighton BN1 9QH
United Kingdom

Summary

The extent to which primary visual cues such as motion or luminance are segregated in different cortical areas is a subject of controversy. To address this issue, we examined cortical activation in the human occipital lobe using functional magnetic resonance imaging (fMRI) while subjects performed a fixed visual task, object recognition, using three different primary visual cues: motion, texture, or luminance contrast. In the first experiment, a region located on the lateral aspect of the occipital lobe (LO complex) was preferentially activated in all 11 subjects both by luminance and motion-defined object silhouettes compared to full-field moving and stationary noise (ratios, 2.00 ± 0.19 and 1.86 ± 0.65, respectively). In the second experiment, all subjects showed enhanced activation in the LO complex to objects defined both by luminance and texture contrast compared to full-field texture patterns (ratios, 1.43 ± 0.08 and 1.32 ± 0.08, respectively). An additional smaller dorsal focus that exhibited convergence of object-related cues appeared to correspond to area V3a or a region slightly anterior to it. These results show convergence of visual cues in LO and provide strong evidence for its role in object processing.

Introduction

The primate visual cortex contains numerous visual areas whose retinotopy, functional characteristics, connectivity, and anatomy have been extensively documented (reviewed by Felleman and Van Essen, 1991; Tootell et al., 1996; Courtney and Ungerleider, 1997; Van Essen and Drury, 1997). However, it remains a matter of debate what organizational principles underlie the specialization of visual areas. In particular, it is still unclear to what extent visual areas segregate the incoming visual information into channels specialized for primary cues such as color, luminance, or motion and to what extent visual areas integrate different visual cues toward performing a specific visual task (for an exposition of this issue, see Ungerleider and Haxby, 1994; DeYoe et al., 1994; Goodale et al., 1994).

Single neuron recordings in the macaque provide evidence both for segregation of visual cues into different channels (Livingstone and Hubel, 1988; DeYoe et al., 1994) and for convergence of several primary cues even at the level of single cortical neurons (Sary et al., 1993). Similarly, studies of anatomical connections indicate the existence of parallel specialized cortical streams (Young, 1992) but also show substantial interstream communication both between areas (reviewed by Felleman and Van Essen, 1991) and in the intrinsic neuronal architecture (Salin et al., 1989; Malach et al., 1995).

Several neuroimaging studies have attempted to address the issue of convergence of cues in the human visual cortex. On the one hand, evidence for convergence of visual cues in specific areas was provided both by Ffytche et al. (1995), who demonstrated that human motion area V5/MT can be activated by motion-from-hue, and by Dupont et al. (1997), who showed that kinetic- and luminance-defined gratings activate a specific human cortical region, Kinetic Occipital (KO). On the other hand, Gulyas et al. (1994) showed that form-from-color stimuli activate a different anatomical region than form-from-motion, suggesting segregation of some visual cues.

In order to further elucidate this fundamental issue, we investigated convergence of cues in object-related areas of the occipital lobe. Recently, it was found that a region located on the lateral aspect of the occipital lobe, termed the lateral occipital complex (LO), is activated preferentially to images of luminance-defined objects as compared to a variety of texture patterns (Malach et al., 1995). In the present study, we examined whether the same preferential activation exists for objects defined solely by motion and texture cues and whether these cues converge on the same cortical sites. Our results show a clear convergence of cues in LO and, surprisingly, reveal that such cue convergence can be found even in earlier, retinotopic cortical sites. Some of these results have been published previously in abstract form (Grill-Spector et al., 1997, Soc. Neurosci., abstract).

Results

Objects from Motion

In this experiment, we directly compared activation to objects defined by luminance cues (objects-from-luminance [OFL]) and motion cues (objects-from-motion [OFM]). Control stimuli consisted of stationary dot patterns (noise [N]) and full-field, uniformly moving dots (motion [Mtn]). The experiment is illustrated in Figure 1 (for details, see Experimental Procedures). To reveal the main activation patterns, we conducted a variety of statistical tests to search for voxels that showed a particular functional profile. We first conducted two tests: one aimed at mapping the distribution of voxels

§To whom correspondence should be addressed.

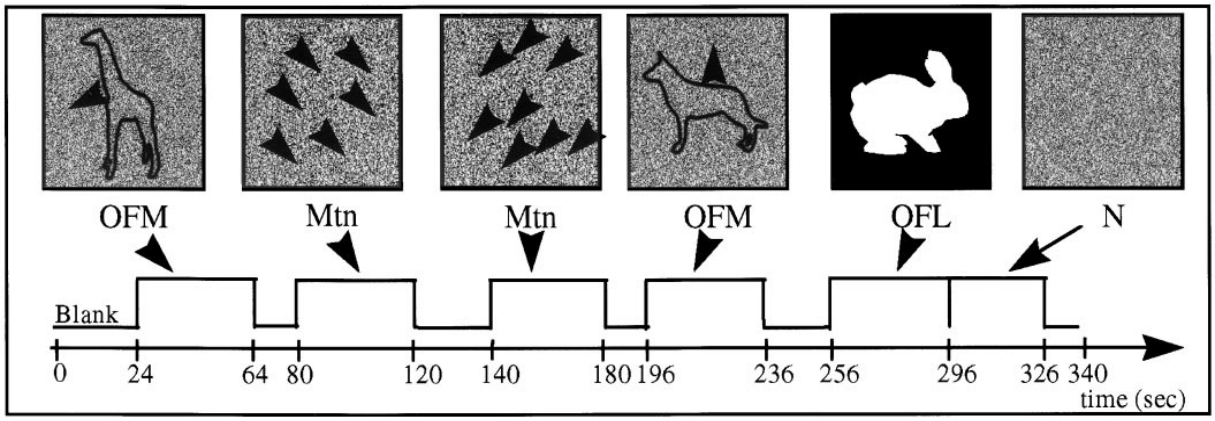

Figure 1. Objects-from-Motion Experiment

Six visual epochs alternated with blank periods. The upper row illustrates the visual stimuli used; the time axis indicates the epochs' length and sequence. The first and fourth epochs displayed objects' silhouettes defined by motion (OFM). The second and third epochs displayed full-field uniform motion (Mtn). The fifth epoch displayed luminance-defined object silhouettes (OFL). The sixth epoch displayed full-field stationary noise patterns (N). The illustrated object boundaries in the OFM epochs indicate kinetic motion contours and not real contours (see Experimental Procedures for more details). Subjects were instructed to covertly name all of the visual stimuli, including images containing nonobjects.

activated by luminance-defined objects (OFL) and the second aimed at mapping the distribution of voxels activated by motion-defined objects (OFM). The first test (OFL test) identified voxels for which the activation in the OFL epoch was significantly higher compared with the activation induced by static or full-field moving noise (OFL $>$ N and Mtn). Epochs consisting of OFM were not considered in this statistical test. This test revealed a bilateral focus of activation in the lateral occipital region of the hemispheres (see pink voxels in Figure 2b, top left) and often (9 of 11 subjects) a smaller focus located more medially and dorsally (cf. dorsal blue voxels depicted in Figure 2c).

The second test revealed voxels that were significantly activated by OFM compared to full-field coherent motion of random dots or static random dots (OFM $>$ Mtn and N). In this statistical test, the OFL epoch was ignored. Two foci of activation were found in both hemispheres: a dorsal focus and a ventral one, as depicted by the turquoise-colored voxels in Figure 2b. Subsequently, the two maps were superimposed to check for overlapping regions. In all subjects, the two maps overlapped in a region located in the lateral occipital part of both hemispheres. This is illustrated in Figure 2b (bottom panel) in which the overlapping voxels are colored in red. This overlap region comprises voxels responding preferentially to object silhouettes defined both by motion and by luminance cues. The number of voxels in the overlap region was 79% $\pm$ 17% (SD) of the number of voxels derived from the OFL test.

To relate these foci of activation to established human visual areas, we mapped in 5 subjects, during the same experimental sessions, the vertical and horizontal meridians (Sereno et al., 1995; DeYoe et al., 1996) using both natural objects or flickering random dots as stimuli (see Experimental Procedures for details). An example of such a map is shown in Figure 2c, which relates voxels preferentially activated by the OFL test (blue) to the horizontal meridian representation (red) and the vertical meridian representation (green). Similar superposition was performed for all other tests in this experiment. Note the typical interdigitated pattern of vertical and horizontal meridian representations that allow a clear definition of retinotopic areas (indicated by arrows). Regarding object-related areas (blue in Figure 2c), the ventral focus lies lateral to the mapped visual meridians; therefore, it corresponds to the essentially nonretinotopic LO (Grill-Spector et al., 1998). The dorsal focus lies lateral to the second dorsolateral vertical meridian representation, which partially overlaps area V3a.

To further differentiate areas that were activated by moving stimuli, we mapped separately voxels that were activated by motion and voxels that were activated specifically by structure-from-motion (SFM). The motion test highlighted voxels (green voxels in Figure 3) that were significantly activated by all moving stimuli compared to all static images (Mtn and OFM $>$ N and OFL). This test revealed foci of activation in V1/V2 (10 of 11 subjects), MT (all 11 subjects), and a few voxels in V3a (8 of 11 subjects). The SFM test highlighted voxels that were specifically activated by OFM and not by any of the other stimuli (OFM $>$ Mtn and N and OFL). As can be seen from Figure 3 (turquoise), the SFM test revealed a small bilateral focus of activation neighboring area MT but lateral and ventral to it in all 11 subjects. Comparing the location of these motion-selective regions to regions sensitive to objects (red voxels in Figure 3) indicates that object areas do not overlap with areas that are purely motion selective.

Average activation time courses derived from each of the functional foci shown in Figure 3 (left) are depicted in Figure 3 (right). For each subject and each test, the region of interest was designated by the statistically significant voxels; for example, the time courses from all of the red voxels in Figure 3 (left) contributed to the subject average time course depicted in Figure 3 (top right). The time course data of each subject were normalized, and the data from 10 subjects were averaged (1

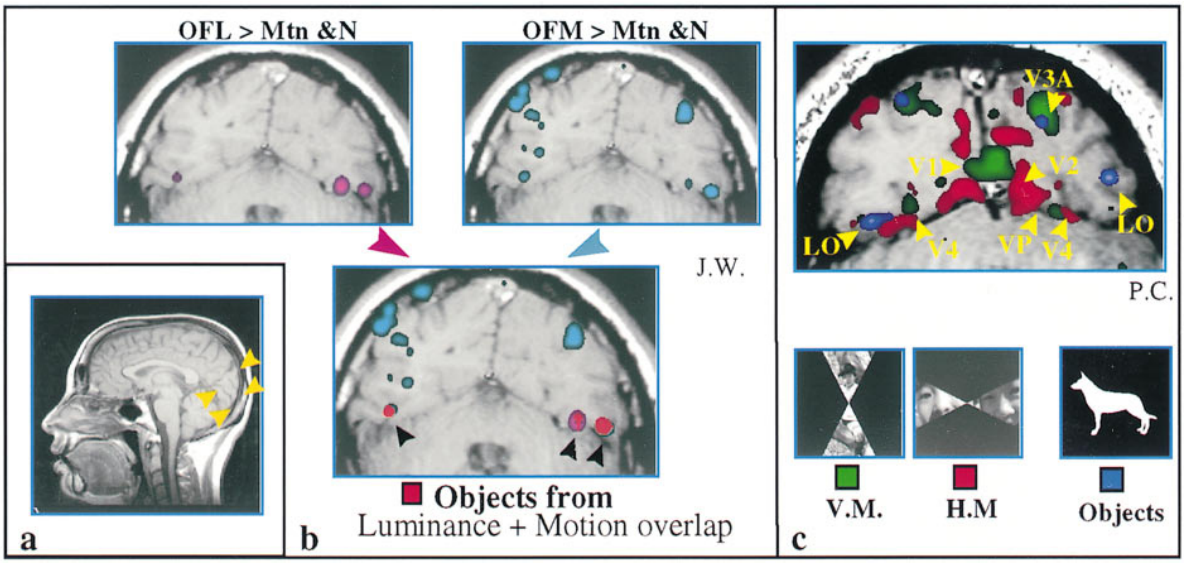

Figure 2. Maps of Object-Related Areas

(a) A mid-sagittal view of the brain. Arrows indicate plane of sections, localized perpendicular to the calcarine sulcus, shown above and in Figures 3, 5, and 6.

(b) Objects-from-motion (OFM) and objects-from-luminance (OFL) maps. An example of the anatomical overlap of areas activated by either OFM or OFL stimuli as compared to activation by motion (Mtn) or static noise (N). The statistical maps were superimposed on a high resolution T1-weighted anatomical section located centrally in the occipital lobe, perpendicular to the calcarine sulcus and parallel to the parieto-occipital sulcus (see [a] for the orientation as indicated by arrows).

(Top left) OFL > Mtn and N. Statistical activation map (pink) showing voxels preferentially activated by object silhouettes compared to static and full-field, coherently moving noise. Epochs of OFM were not considered in this test. Voxel brightness corresponds to the correlation value ρ (darkest $\rho = 0.37$, $P < 1e-8$; brightest $\rho = 0.62$).

(Top right) OFM > Mtn and N. Activation map (turquoise) showing voxels preferentially activated by OFM compared to full-field uniform motion and static noise; the OFL epoch was ignored. The brightness corresponds to the correlation coefficient (darkest $\rho = 0.43$, $P < 1e-5$; brightest $\rho = 0.71$).

(Bottom) Superposition of the two upper maps; the overlap region is colored in red. Note that the overlapping voxels appear ventrally in the lateral occipital region, indicating coactivation by OFL and OFM. The nonoverlapping areas from the OFM > Mtn and N test are probably motion areas activated by relative motion or kinetic boundaries.

(c) Superposition of the OFL test and boundaries of visual retinotopic areas. Superposition of three activation maps showing preferential object activation (blue) and horizontal (red) and vertical (green) meridian representation overlaid upon a high resolution T1-weighted anatomical scan. Section plane is similar to that shown in (a). The borders of retinotopic visual areas, indicated by arrows, were delineated by the vertical and horizontal meridians. Blue voxels indicate regions in which activation by OFL was more pronounced compared to activation by full-field static and moving noise. Note that the ventral blue focus is located outside the retinotopic borders, indicating correspondence to the essentially nonretinotopic LO. The dorsal blue focus is located in a retinotopic region overlapping or near area V3a.

subject was not included because the order and timing of the epochs in his scan were different). To provide a quantitative summary of the activation profiles, we also calculated the activation ratios for each region (see Experimental Procedures for details). In all 11 subjects, the OFL test, which picked voxels solely according to their preferential activation to luminance-defined static silhouettes, revealed a preferential activation both to luminance and motion-defined objects (see Figure 3, top right, and Table 1, top row). We carefully examined LO for voxels that were activated purely by luminance-defined objects and not by motion-defined objects. This detailed examination revealed that only a small minority (11% $\pm$ 8% [SD]) of such voxels existed in LO. In 7 of 11 subjects, these few voxels were located in the ventral aspect of LO, whereas in 2 subjects, no such voxels were detected.

Regions activated specifically by OFM showed a marked reduction in activation to uniform moving noise, and an even stronger reduction to static noise (see Figure 3, center right, and Table 1, SFM). Finally, motion-related areas responded more strongly to moving stimuli compared to static stimuli. As evident from Table 1, both OFM and full-field moving noise stimuli produced a signal almost twice as large as the signal evoked by static images, of either objects or noise. Motion-related areas showed some heterogeneity in the relative signal of the Mtn epoch compared to the OFM epoch (both epochs contain moving stimuli). Analyzed separately, V1 voxels activated slightly more to full-field motion compared to OFM, whereas MT voxels behaved in an opposite manner (data not shown).

Additional Controls

The results presented so far point clearly to convergence of luminance and motion cues in defining objects in LO. However, it could be argued that there are confounding factors in the experiment that may lead to alternative interpretations. Among these factors, three are of particular concern.

Eye Movements

One possibility is that different patterns of eye movements occurred in the epochs containing objects compared to the noise epochs, and that the activation in LO

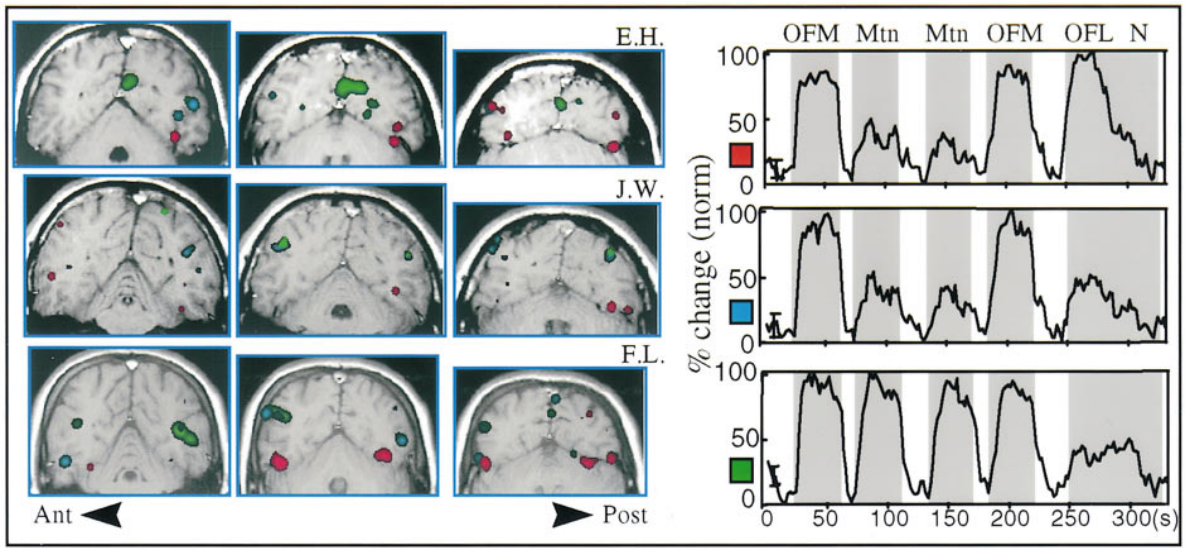

Figure 3. Objects-from-Motion Experiment

(Left) Activation maps. Superposition of the activation maps of the different foci of activation in the OFM experiment of three different subjects (each row depicts three consecutive slices of a single subject, where the rightmost column depicts the most posterior slice). Colored voxel brightness corresponds to the correlation coefficient (darkest $\rho = 0.37$, $P < 1e-8$; lightest $\rho = 0.9$). The corresponding time courses for each of these activation foci are displayed on the right.

(Right) Time courses. Average time courses of 10 subjects derived from the OFM experiment. The x-axis denotes time in seconds, and the y-axis shows normalized fMRI signal strength. Error bars denote ± 1 averaged SEM. Abbreviations: OFM, objects-from-motion; Mtn, full-field motion; OFL, objects-from-luminance; N, stationary noise patterns. Shaded epochs indicate visual stimulation; unshaded epochs indicate blank epochs. Time courses were derived from the most significant voxels for each test. Examples of the corresponding activation maps from which these time courses were derived are shown on the left.

(Red) OFL test. Voxels (left) and corresponding time course (right) that were activated more by luminance silhouettes (OFL) compared to full-field motion of random dots (Mtn) or static noise (N) epochs. OFM epochs were ignored. Note that although OFM epochs were excluded from the statistical test, voxels that were selectively activated by OFL were also activated by OFM. This indicates convergence of both motion and luminance cues within these voxels. The mean number of voxels per subject that was used for the subject average time course was 180 ± 94 voxels.

(Turquoise) SFM test. Voxels that were significantly activated by OFM compared to full-field motion (Mtn) or static images (OFL and N). Mean number of voxels per subject, 50 ± 38 voxels.

(Green) Motion test. Voxels that were significantly activated in epochs containing moving visual stimuli (OFM and Mtn) compared to static images (OFL and N). Examples of the anatomical location of these voxels are presented on the left and correspond to the green-colored voxels. The mean number of voxels per subject, 177 ± 56 voxels.

was affected by these eye movements. To address this issue, we conducted a control experiment in which a small fixation point was placed at the center of the image. The subjects' task was to fixate throughout the experiment, while naming the images.

Unbalanced Movement Vectors

It could be argued that the full-field moving dot epoch was not a good control for the OFM epoch, since in the latter a large part of the image (the background) was stationary. If LO was somehow inhibited by motion, the preferential activation during the OFM epoch may have been a consequence of the fact that a lesser number of dots were moving during that epoch compared to the full-field motion epoch. To address this point, we conducted a control experiment comparing an OFM epoch that contained a stationary background with an OFM epoch in which all dots were moving: the object silhouette in one direction and the background in the opposite direction.

Structure-from-Motion but Not Object-from-Motion

Finally, the preferential activation by OFM might have resulted from a nonspecific activation by second order

Table 1. Average Activation Ratios of the OFM Experiment

	OFL/N	OFM/N	Mtn/N	OFM/OFL
OFL test	2.00 ± 0.19*	1.86 ± 0.65*	1.01 ± 0.31	0.90 ± 0.06
SFM test	1.60 ± 0.15*	2.80 ± 0.33*	1.55 ± 0.19*	1.73 ± 0.08*
Motion test	1.00 ± 0.08	1.87 ± 0.15*	1.91 ± 0.15*	1.88 ± 0.14*

Ratios were calculated for 11 subjects. They were derived from the OFL test (Figure 3, red voxels), SFM test (Figure 3, turquoise voxels), and motion test (Figure 3, green voxels). See the Experimental Procedures for details of the ratio calculations. Values denote the means $\pm$ SEM. Abbreviations: OFL, objects-from-luminance; OFM, objects-from-motion; Mtn, full-field coherently moving dots; N, static full-field noise. Asterisks denote ratios that are significantly greater than 1 ($\alpha < 0.01$).

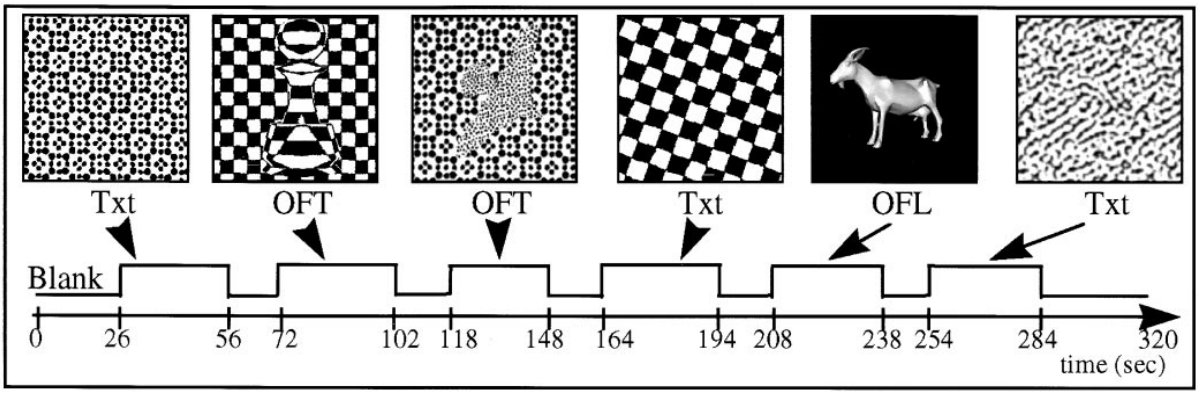

Figure 4. Objects-from-Texture Experiment

The upper row illustrates the visual stimuli used in the experiment, and the time axis indicates the epochs' length and sequence. Images were presented at a rate of 0.5 Hz; visual epochs were alternated with blank epochs. In the first, fourth, and sixth epochs, 15 different textures (Txt) were presented randomly. The second and third epochs consisted of 15 images of animals or man-made objects created by texture contrasts (OFT). The fifth epoch consisted of gray-level luminance-defined objects (OFL) from the same categories. In the first OFT epoch, both the object and background consisted of the same texture, while in the second OFT epoch, the object and the background consisted of different texture patterns. Note that boundaries in OFT epochs are subjective boundaries created at texture borders. Subjects were instructed to covertly name all of the visual stimuli, including the texture patterns.

motion and not by the presence of objects defined by motion. To address this concern, we contrasted epochs containing motion-defined object silhouettes (OFM) with epochs containing motion-defined square wave gratings (gratings-from-motion, GFM). This test was relevant, since it had been found previously (Malach et al., 1995) that LO shows preferential activation to luminance-defined objects versus gratings.

The results of the control experiments, conducted on 8 subjects, were clear-cut and further strengthened the conclusion that both motion- and luminance-defined objects preferentially activate LO. Thus, preferential object selectivity for luminance- and motion-defined objects compared to luminance- and motion-defined gratings was evident when subjects were fixating (ratio, 1.62 ± 0.13, SEM), indicating that eye movements could not account for the results. The preferential activation of LO to objects when the background was moving in the opposite direction from the silhouettes was actually slightly enhanced (ratio, 1.10 ± 0.05, SEM) compared with activation to silhouettes moving over a stationary background, ruling out different numbers of moving dots as the confounding factor. Finally, motion-defined object silhouettes (OFM) activated LO preferentially compared with motion-defined gratings, albeit with slightly less contrast (ratio, 1.52 ± 0.09, SEM) compared to noise patterns. This result rules out the possibility that the preferential activation during the OFM epoch was due to nonspecific, second order motion activation.

Objects from Texture

In this experiment, we extended the question of convergence to another cue that can be utilized to define objects: texture contrast. Thus, we tested whether texture contrasts defining an object form will activate visual object-related areas. Visual stimulation consisted of ojects-from-texture (OFT) images, uniform black-and-white textures (Txt) and gray-level, three-dimensional luminance-defined objects (objects-from-luminance, OFL). An illustration of the experiment is depicted in Figure 4 (for details, see Experimental Procedures).

In analyzing the results of this experiment, we performed three statistical tests. The first test (objects) used the established "signature" of object-related areas (Malach et al., 1995) and highlighted voxels that showed increased activation to luminance-defined objects compared to pure textures (OFL $>$ Txt). In this test, the OFT epochs were not considered. In the second test, we searched for voxels that had higher activation in the OFT epochs compared to textures (OFT $>$ Txt), and in this case the OFL epoch was ignored. Both of these tests revealed similar foci of activation (e.g., the red voxels in Figure 5a indicate the overlap region of the OFL and OFT tests in 1 of the subjects). This suggests that areas that displayed increased activation by luminance-defined objects showed also increased activation by OFT when compared to uniform textures. The number of voxels in the overlap region was 75% $\pm$ 12% (SD) of the number of voxels defined by the OFL test. Previous studies have indicated a slight bias to texture activation in early visual areas (Malach et al., 1995); thus, we conducted a third test (textures) aimed at revealing preferential activation to uniform textures compared to objects (Txt $>$ OFL).

Figure 5b shows an example of the activation maps for the object and texture tests for 1 subject. The red voxels are the statistically significant voxels of the objects test (OFL $>$ Txt). The blue voxels are those voxels that respond preferentially to textures compared to luminance objects (Txt $>$ OFL). It is clear from Figure 5b that areas that were preferentially activated by textures are located medially. Comparing these foci of activation to established area borders suggests that these foci correspond to primary visual areas V1, V2, and a less significant focus in V3 (preferential activation by textures was detected in V1 in all subjects, whereas activation of either V2 or V3 was detected in 9 of 11 subjects). The objects test highlighted a bilateral focus of activation in

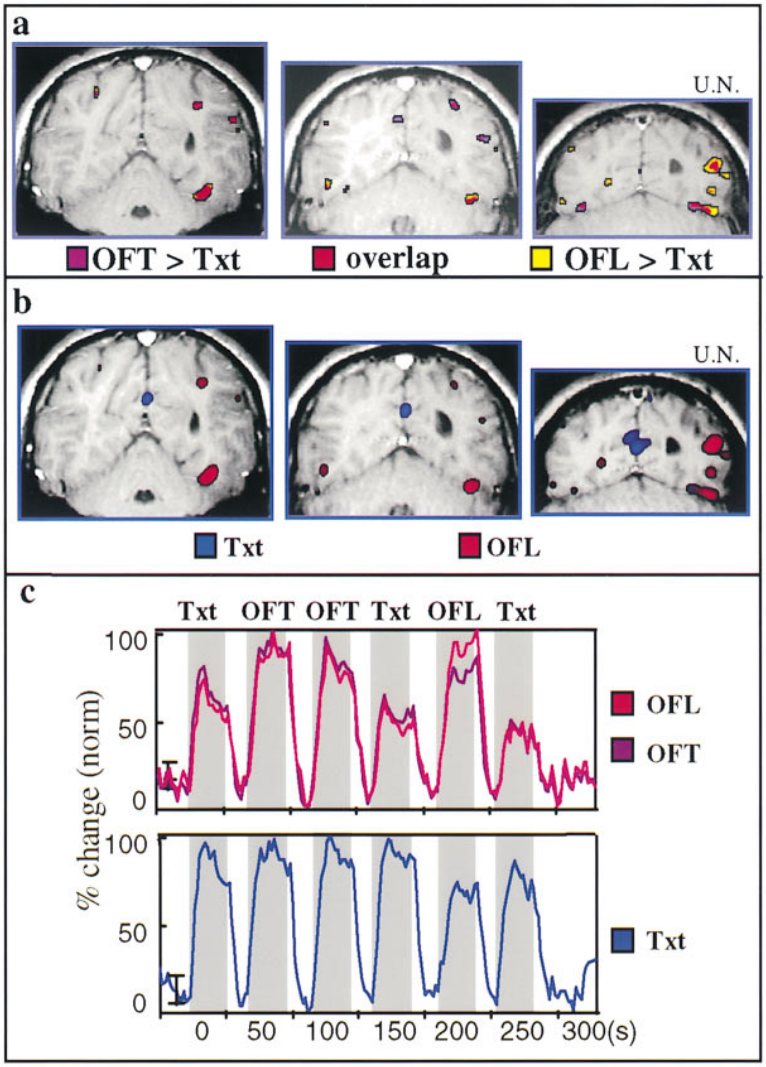

Figure 5. Objects-from-Texture: Activation Maps and Corresponding Time Courses

(a) Overlap of areas activated by either OFT or OFL stimuli. The statistical maps of a single subject, superimposed upon high resolution T1-weighted anatomical sections. Same plane of sections as in Figure 2a.

(Yellow) Activation map showing voxels that were preferentially activated by luminance-defined objects compared to full-field texture patterns; epochs of OFT were ignored ($\rho > 0.49$, $P < 1e-7$). (Purple) Voxels that were preferentially activated by OFT compared to full-field texture patterns; the OFL epoch was ignored ($\rho > 0.4$, $P < 1e-7$).

(Red) Overlap region between the two superimposed maps. Note that an extensive overlap region appears in the LO region, and there is also a smaller dorsal region where these maps overlap. This indicates coactivation in these areas by OFL and OFT.

(b) Comparison of object- and texture-activated regions. Superposition of two activation maps of the foci of activation in the structure-from-texture experiment of three consecutive slices of a single subject. Colored voxel brightness corresponds to the correlation value.

(Red) OFL. Object-related areas activated preferentially by pictures of luminance-defined objects compared to texture patterns. OFT stimuli were not considered in this test ($\rho > 0.49$, $P < 1e-7$).

(Blue) Txt. Areas activated preferentially by textures compared to objects. Note that voxels responding preferentially to textures were located medially compared to voxels activated by objects ($\rho > 0.37$, $P < 1e-6$).

(c) Subject average time courses ($n = 6$) of the OFT experiment. The x-axis denotes time in seconds, and the y-axis shows normalized fMRI signal amplitude. Error bars denote ± 1 SEM. Abbreviations: OFT, objects-from-texture; Txt, texture; OFL, three-dimensional objects-from-luminance. Shaded epochs indicate visual stimulation; unshaded regions indicate blank epochs.

(Red) OFL. Time course derived from voxels identified by a test of preferential activation to luminance-defined objects (OFL) compared to textures; OFT epochs were not considered in the test. An example of the cortical regions from which this time course was derived is shown in (b) (red voxels). Note that although OFT epochs were ignored in the statistical test, voxels that were activated preferentially by luminance-defined objects were also activated concurrently by the OFT stimuli, and not by full-field textures. This indicates convergence of luminance and texture cues that are used to define the objects in these voxels. The mean number of voxels per subject, 145 ± 57 voxels.

(Purple) OFT. Time course derived from a statistical test targeted to identify voxels that were activated preferentially by texture-defined objects (OFT) compared to textures. The OFL epoch was ignored in the test. An example of the cortical regions from which this time course was derived is shown in (a) (purple voxels). Note that, overall, the time course derived from this test is similar to the one derived from the OFL test with some invasion into lower order areas. Mean number of voxels per subject, 217 ± 53 voxels.

(Blue) Txt. Time course derived from voxels identified by a test of preferential texture activation compared to objects. OFT epochs were ignored in the test. An example of the cortical regions from which this time course was derived are shown in (b) (blue voxels). Note the similar level of activation in the uniform texture and OFT epochs in these voxels. Mean number of voxels per subject, 123 ± 43 voxels.

LO (all subjects) and a smaller, slightly less statistically significant focus, located dorsally, in what we suspect to be either V3a or a more anterior area adjacent to it (in 5 subjects, the dorsal activation was visible in the right hemisphere; in 3 subjects, the activation was restricted to the left; and 3 subjects showed bilateral activation).

Average time courses were calculated for 6 of 11 subjects (see Figure 5c). The other subjects were not included in the average time course because the sequence of epochs was varied between experimental sessions; however, they showed similar activation patterns. The corresponding activation ratios of all 11 subjects are given in Table 2. It is important to note that

Table 2. Average Activation Ratios of the OFT Experiment

	OFL/Txt1	OFT/Txt1	Txt2/Txt1	Txt3/Txt1	OFT/OFL
Objects	1.43 ± 0.08*	1.32 ± 0.06*	0.80 ± 0.06†	0.72 ± 0.06†	0.93 ± 0.03
Texture	0.76 ± 0.04†	1.02 ± 0.04	0.96 ± 0.07	0.82 ± 0.06†	1.38 ± 0.07*

Ratios were calculated for 11 subjects. They were derived from object (Figure 5, red voxels) and texture (Figure 5, blue voxels). See the Experimental Procedures for details of the ratio calculations. Values denote the means ± SEM. Abbreviations: OFL, object-from-luminance; Txt, full-field textures (the number indicates the serial number of the texture epoch); OFT, object-from-texture. Asterisks denote ratios that are significantly greater than 1 ($\alpha < 0.01$). Daggers denote ratios that are significantly smaller than 1.0 ($\alpha < 0.01$).

similar to the OFM experiment, object-related voxels were defined solely according to their preferential activation to luminance-defined objects. Nevertheless, their time course revealed a significant increase in activation also in the OFT epochs. This indicates convergence of luminance and texture cues that define objects on individual voxels. Primary areas showing preferential activation to textures compared to luminance objects were activated by OFT to the same extent as plain textures.

Another phenomenon that is evident from the average time course (see Figure 5c) is the decline of the activation to the textures during the course of the experiment, both in object-related areas and in texture-dominated areas (compare the ratios of Txt2/Txt1 and Txt3/Txt1 given in Table 2). The source of this reduction is still not clear. It should be noted that different textures were presented randomly in the three texture epochs, but all epochs contained similar types of texture patterns such as checkerboards, dot patterns, and so on.

Combining the OFM and OFT Experiments

In both the OFM and OFT experiments, a luminance-defined object activation was associated with an additional visual cue; thus, it is expected that the OFT and OFM cues will also be associated with each other. Since somewhat different luminance-defined objects were used in the two experiments, we superimposed the maps obtained for object-related areas in the OFM experiment (light blue voxels in Figure 6) with those obtained in the OFT experiment (yellow voxels in Figure 6). The results of this superposition in 9 subjects are shown in Figure 6. As can be seen, there was a substantial overlap (red voxels in Figure 6) in the bilateral LO region. The dorsal focus also displayed the same functional overlap (e.g., subject OC in Figure 6). Considering the variability encountered between experiments, it is most likely that these comparable regions represent the same cortical areas. The corresponding Talairach coordinates of these foci are given in Table 3. It should be noted that the anatomical extent of LO as defined in the present experiments is similar to that found in the original studies (Malach et al., 1995; Tootell et al., 1996).

Finally, regarding the issue of lateralization, LO activation was evident in both hemispheres in all subjects, and there appeared to be no correlation between lateralization and subject's right or left handedness. In 10 of 11 subjects, there was a right hemisphere bias in the two most anterior sections (mean number of voxels in

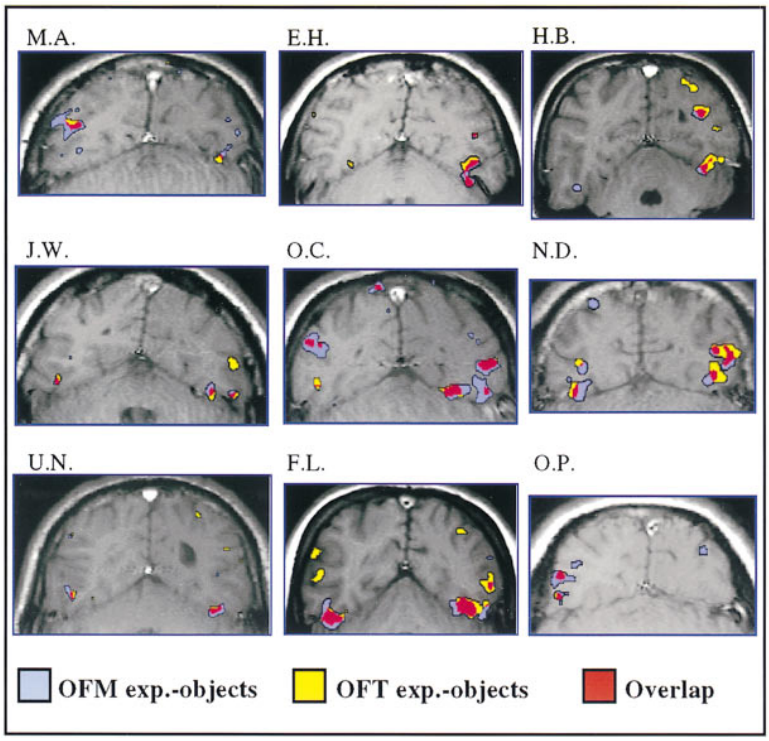

Figure 6. Comparison of OFT and OFM Object Area Activation Maps

Superposition of activation maps obtained by testing for voxels activated preferentially by luminance-defined silhouettes compared to random dots in the OFM experiment (light blue; $P < 1e-6$) and by luminance-defined objects compared to texture patterns in the OFT experiment (yellow; $P < 1e-6$). Regions of overlap of the OFM and OFT experiments were colored in red. The maps were overlaid upon T1-weighted high resolution anatomical sections oriented similarly to the plane indicated by the arrows in Figure 2a. The figure depicts one representative slice per subject. Note the extensive overlap of these maps located bilaterally, corresponding to LO. A smaller focus was located dorsally and possibly corresponds to area V3a or to a neighboring area (e.g., subject O. C.). Note that these regions of overlap consist of voxels that were activated by objects defined by luminance, motion, or texture.

Table 3. Talairach Coordinates

	Left			Right		
	x	y	z	x	y	z
LO	−41 ± 6mm	−75 ± 9mm	4 ± 2mm	37 ± 7mm	−71 ± 6mm	4 ± 3mm
	−39 ± 6mm	−68 ± 7mm	−13 ± 5mm	41 ± 6mm	−67 ± 9mm	−14 ± 3mm
	−39 ± 7mm	−53 ± 5mm	−12 ± 6mm	33 ± 4mm	−45 ± 7mm	−14 ± 8mm
V3a?	−21 ± 5mm	−76 ± 7mm	23 ± 8mm	25 ± 5mm	−73 ± 4mm	23 ± 6mm

Talairach coordinates (Talairach and Tournoux, 1988) were calculated for 9 subjects. They were derived from regions that exhibited convergence of objects-from-luminance, objects-from-motion, and objects-from-texture (see Figure 6). The LO complex can be bounded by three vertices: the first row corresponds to the dorsal posterior vertex, the second to the ventral posterior vertex, and the third to the ventral anterior vertex. The fourth row denotes the coordinates of the center of the V3a focus. Values represent the mean ± SD in millimeters.

left anterior slices = 8 ± 9 voxels and in right anterior slices = 23 ± 12 voxels; ratio, left/right = 0.39 ± 0.42 [SD]). Two of these 10 subjects showed a right hemisphere bias in all slices.

Discussion

Convergence of Cues

The central finding of the present study is that different visual cues converge in object-related areas; that is, motion, texture, and luminance contrasts can activate object-related areas as long as they are used in the definition of object forms. This conclusion is derived first from the overlap in activation maps, such as in Figures 2b and 5a, which show anatomical overlap of activation maps for different cues, but more conclusively by the activation time course data (Figures 3 and 5c). These time courses were obtained from voxels that were defined solely by their preferential activation to luminance-defined objects, and yet they concurrently show clear activation for motion- and texture-defined objects. Thus, the preferential activation to luminance-defined objects and the motion and texture cues occurs at the level of individual voxels. Given that the resolution of the functional magnetic resonance imaging (fMRI) technology is a few millimeters, this strongly suggests the convergence of cues within individual visual areas. Whether or not the convergence occurs at the single neuron level, as has been shown for macaque IT (Sary et al., 1993), remains to be seen. Thus, our study strongly supports the notion that cortical areas can utilize a diverse array of visual cues in the performance of visual tasks.

Comparison to Related Studies

The results of the OFM experiment are in line with evidence that letters generated by structure-from-motion activate LO (Goebel et al., 1997, Neuroimage, abstract). It should be noted that we have not tested letter stimuli directly, and it may be that letters have a distinct representation (Puce et al., 1996; Tanaka, 1997). Other studies report that GFM did not appear to activate LO but rather another area, KO (Dupont et al., 1997), while motion boundaries seem to activate only low order areas (Reppas et al., 1997). The results of the control OFM experiment are in agreement with these studies in showing preferential activation of LO voxels by objects compared to gratings, regardless of the visual cue. This indicates that the enhanced LO activation is probably not due to a general response to surfaces, or to second order motion, but requires sufficiently complex natural objects.

Concerning the OFT experiment, one possible interpretation of the results of enhanced activation in the OFT epoch is that subjective contours are the shape-defining feature in these stimuli. This is compatible with reports of selective activation to subjective contours in LO (Mendola et al., 1997, Neuroimage, abstract) and even in lower order areas (Hirsch et al., 1995).

V3a?

We consistently found in both the OFM and OFT experiments a small focus of activation located dorsally. This focus was partially situated within a retinotopic region (unlike LO, which appears to be nonretinotopic; Grill-Spector et al., 1998) but in these experiments had a similar activation profile to LO. Superimposing the foci of activation and maps of vertical and horizontal meridians of the visual field suggests that this focus partially overlaps area V3a (see Figure 2c). It should be noted that in the anterior slices the meridian mapping is quite sparse and complex; therefore, our identification of the anterior limit of this focus is tentative.

fMRI studies in humans have mapped the retinotopic characteristics of V3a (Sereno et al., 1995; DeYoe et al., 1996; Tootell et al., 1997), showing clear homology to macaque V3a. On the other hand, unlike the macaque, human V3a (but not V3) is sensitive to moving stimuli (Tootell et al., 1997), suggesting its relation to the magnocellular stream. Our results extend the functional characterization of human V3a by showing that it may also be associated with object processing.

KO/STP

The OFM experiment revealed two bilateral foci in the lateral portion of the hemisphere in which the activation was increased by OFM compared to full-field motion. One focus corresponded to LO and the other focus was situated dorsally, adjoining MT but located more laterally and ventrally. This dorsal focus might correspond to a recently reported motion area, Kinetic Occipital (KO) (Orban et al., 1995; Dupont et al., 1997), that responds both to kinetic and luminance gratings. In our study, OFM produced the maximal signal in this area, but both moving noise and object silhouettes produced a slight enhancement of the fMRI signal compared to static

noise (see activation ratios in Table 1). Another possibility is that the observed functional profile does not represent a separate visual area but is caused by sampling from voxels bordering both areas MT and LO.

Object Recognition in the Occipital Lobe

Our results are also relevant to the issue of object recognition in the human occipital lobe. The present study, as well as other neuroimaging studies showing selective activation to various object categories (Haxby et al., 1996; Martin et al., 1996; Puce et al., 1996; Kanwisher et al., 1997a, 1997b), used natural objects such as animals, faces, and man-made objects, which proved to be optimal for activating several high level primate cortical areas (Malach et al., 1995; Tanaka, 1996). However, these complex stimuli cannot be easily defined by a limited set of quantitative parameters. Therefore, it is difficult to deduce what features of object stimuli generated the activation in these high order areas and consequently to demonstrate the role of these areas in object representation. This problem is less acute for single unit recording in macaque monkey (Logothetis and Sheinberg, 1996; Tanaka, 1997). Our controls ruled out many of the potential confounding factors such as eye movements, imbalance in the extent of motion, and nonspecific second order motion effects (see Results and Table 1). However, other low level factors may still account for the results of each experiment when considered separately. The present study circumvents this inherent difficulty by demonstrating a convergence of visual cues that are unrelated except for their utilization in defining object form. We emphasize that the main outcome of the present study is not the finding of preferential activation for each individual visual cue; rather, it is the demonstration of convergence of such object-related cues, indicating a clear role for LO in object representation.

Experimental Procedures

General Procedure

Thirteen healthy volunteers (ages 22–40, 7 female) who gave written informed consent participated in the study. The experimental protocol was approved by the Chaim Sheba Medical Center ethics committee. The fMRI measurements were performed in a whole-body MRI system (2T Prestige, Elscint) operating at a magnetic field of 1.9 Tesla and equipped with a standard birdcage head coil. Functional data were obtained using a susceptibility-sensitive EPI pulse sequence (a T2*-weighted multislice gradient echo sequence; TR/TE/flip angle = 2000/45/90°) with FOV of 38.4 × 19.2 cm^2, matrix size of 128 × 72, and in-plane resolution of 3 × 2.7 mm. A typical session began with a sagittal scan, on which six slices, 6 mm thick, were selected such that they covered most of the occipital lobe. The slices were localized on the midline sagittal slice oriented approximately perpendicular to the calcarine sulcus and parallel to the parieto-occipital sulcus (see Figure 2a). The sagittal scan was followed by a high resolution (0.8 mm × 1.5 mm × 5 mm) standard structural T1-weighted anatomical scan. Prior to the functional scans, an interactive shimming procedure was applied individually for each subject.

Experimental Protocol

Visual stimulation was generated on an SGI workstation and was back-projected via an LCD projector onto a screen located at the back of the scanner. Subjects viewed the stimuli through a mirror attached to the head coil, providing a maximal field of view of 40° horizontally × 30° vertically. Images in this study subtended a visual angle of 30° horizontally × 30° vertically. The average luminance of the images was 80 candela/m^2, with blanks at 20 candela/m^2. A typical experimental session included six to eight functional scans (each consisting of a different experiment) lasting 5:20–5:40 min, such that the total measurement time was ~1–1.5 hr. Each functional scan generated a total of 960–1020 images collected over 320–340 s from six contiguous slices of the brain. The first four image acquisitions were discarded. A total of 13 subjects were scanned, but two scans in which head motion exceeded several voxels were rejected.

Visual Stimuli

Objects-From-Motion (OFM) Experiment

Epochs of visual stimulation 40 s long were alternated with 16 or 20 s blank epochs. Examples of the pictures presented in each epoch are shown in Figure 1. In this experiment, all epochs but one consisted of black and white random dot (noise) patterns that were previously shown (Malach et al., 1995) to produce a weaker activation compared to pictures of natural objects in object-related areas. Two OFM epochs were created by coherently moving a section of the noise pattern over the stationary background, creating an image of a drifting object silhouette (see Figure 1, OFM). Motion (Figure 1, Mtn) epochs consisted of full-field coherent motion of similar noise patterns. These control epochs were used to differentiate areas selectively activated by moving stimuli such as area MT (Dupont et al., 1994; Tootell and Taylor, 1995; Tootell et al., 1995). Dots moved in a straight trajectory in both the Mtn and OFM epochs at a speed of ~2°/s. The visual patterns as well as their direction of motion were changed at a rate of 0.3 Hz. One epoch (Figure 1, OFL) contained stationary white animal silhouettes displayed upon a black background, and one epoch (Figure 1, N) contained stationary full-field noise patterns. Stationary images were alternated every 2 s.

Subjects were asked to covertly name all of the visual stimuli, including images of nonobjects. Subsequent to the scan, subjects viewed the experiment a second time and indicated which objects were recognized in the scanning session. Essentially, all objects were easily recognized in all conditions. Three subjects could not identify 1 of 18 animals presented in the OFM epoch, whereas other subjects recognized all objects. In the luminance-defined object epoch, subjects had 100% recognition rate. Typical "names" given to the nonobject stimuli, which are illustrated in Figure 1, were dots moving left, black dots moving to the right, many black dots, etc. Three subjects were also instructed to recall names of animals in the second blank epoch to control for pure naming activation (without visual stimuli).

Control (OFM) Experiment

In this control experiment, we examined the potential effects of eye movements, unbalanced number of moving dots, and nonspecific SFM. Epochs of visual stimulation of 40 and 30 s long were alternated with 16 s blank epochs, of similar average luminance. The visual patterns as well as their direction of motion were changed at a rate of 0.3 Hz. Subjects were instructed to fixate upon a small red fixation cross (0.3°) while covertly naming all of the visual stimuli. In this experiment, OFL and OFM were contrasted with GFL and GFM.

The experiment consisted of two OFM epochs: the first OFM epoch was similar to the previous experiment, while in the second OFM epoch both background and objects moved but in opposite directions. The relative speed between the foreground and the background remained the same (2°/s) in the two epochs. Gratings epochs consisted of square gratings of width and spacing in the range of 0.7°–2.7° in various orientations (0, ±30, ±45, ±60, 90). GFM were created similar to OFM (see above), except that here the drifting silhouettes were shaped as square wave gratings. One epoch (OFL) contained stationary white animal silhouettes displayed upon a black background, and one epoch (GFL) contained stationary black-and-white gratings of the same type that were used in the GFM epoch.

Objects-From-Texture (OFT) Experiment

Epochs of stationary visual stimulation 30 s long were alternated with 16 s blank epochs (see Figure 4); the number and order of blank epochs were altered in several versions of this experiment. In this experiment, all epochs but one consisted of images containing black and white textures. The textures in the various epochs were pooled from a set of texture patterns (dots, checker-boards, etc.)

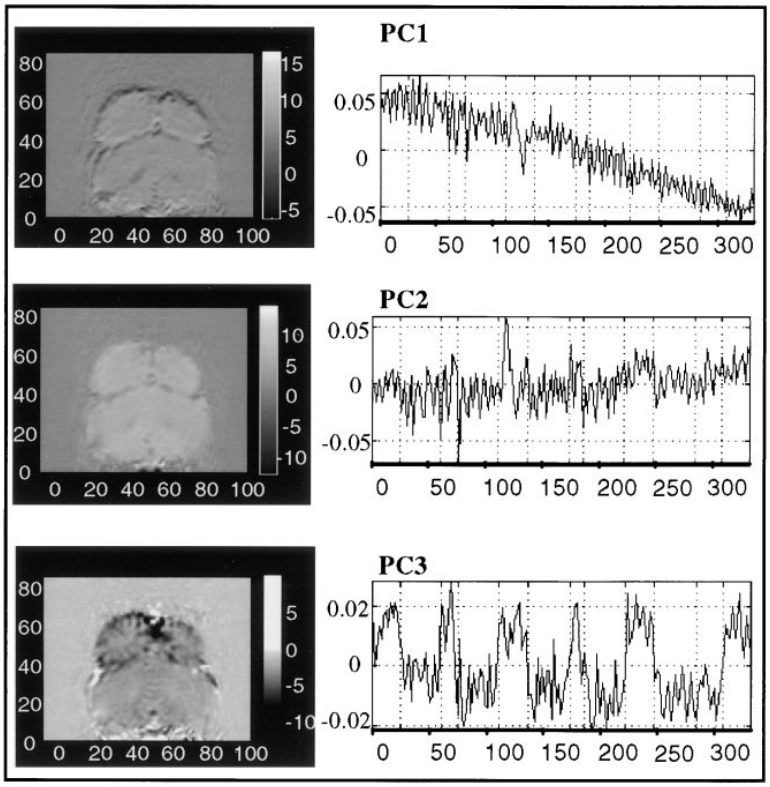

Figure 7. PCA Preprocessing

An example of the PCA preprocessing stage on one slice of subject F. L. in the OFM experiment. The orthonormal principal components (PCs) of a user-selected ROI were calculated and depicted in decreasing order of their significance (see Appendix for details).

(Right) The three most significant principal components. The x-axis denotes time in seconds, and the y-axis denotes the PC amplitude. (Left) Gray level maps showing the distribution of the principal component scores within the slice (brightness corresponds to the amplitude of the component). White denotes positive values and black denotes negative values. In this example, the first and second principal components (PC1 and PC2) were discarded prior to statistical analysis; the third component (PC3) depicts the visual signal (inverted) component, which was not removed.

(Top) The most significant component depicts a slow drift. Note that this component is emphasized on slice boundaries.

(Center) High frequency correlated noise component. Note the even distribution of this component across the entire slice.

(Bottom) The visual signal component. The principal component is inverted; hence, times in which the component is negative correlate to times when a visual stimulus was presented. Anatomically, this component is emphasized (black) in the medial and lateral portions of the cortex.

available in the SGI Inventor Mentor libraries and from textures generated by rotating and skewing these basic patterns. One epoch (OFL) contained three-dimensional computer-generated objects (man-made objects and animals, from the three-dimensional library of Viewpoint Data Labs) depicted in 256 gray levels, and two epochs contained objects from the same categories formed by texture contrast (OFT) as depicted in Figure 4. OFT images were formed by wrapping a texture around a three-dimensional computer-generated object and filling the background with a flat texture. In the first OFT epoch, both the object and background contained the same texture and the object was visible by the distortion of the texture when wrapped around the object. In the second OFT epoch, the same procedure was applied to create the images, except that the object and the background consisted of different texture patterns. It should be noted that uniform texture patterns provide suboptimal activation of area LO (Malach et al., 1995).

Subjects were instructed to covertly name all of the visual stimuli, including images that did not contain objects. Subsequent to the scan, subjects were presented with the experiment for a second time and asked to indicate the recognizable objects. Only one subject had difficulty identifying the objects in the first OFT epoch, while the other subjects had a recognition rate of 100% in all conditions. Typical "names" given by the subjects to the texture patterns that are depicted in Figure 4 were black dots, checkerboard, worms, and so on.

Mapping Borders of Visual Areas

To delineate the borders of retinotopic areas, the representations of the vertical and horizontal visual field meridians were mapped (Sereno et al., 1995; DeYoe et al., 1996). Visual stimuli presented at a rate of 2 Hz consisted of horizontal or vertical wedge shapes (see Figure 2c) to compensate for the expanded foveal representation. A small fixation cross (0.56°), whose color changed randomly, appeared in the center of the image. Subjects were instructed to fixate upon the cross and covertly name its color. Half of the wedges were made of gray-level natural images cropped to fit the wedge shape, and the other half were made of flickering black and white random dots. The flickering dot stimuli were effective in mapping the borders of V1 and V2, while the natural images were optimal in revealing higher order areas, i.e., the vertical meridians at the border between areas VP and V4v (ventrally) and V3 and V3a (dorsally) and the horizontal meridians defining the borders of V4v and V3a (Sereno et al., 1995; DeYoe et al., 1996; Tootell et al., 1997).

Data Analysis

All data were analyzed offline using programs that were developed using the MATLAB 4.2c software package (MathWorks, Natick, MA). The MATLAB programs were compiled to decrease processing time. The main stages in data analysis are outlined below.

Preprocessing

One of the concerns in analyzing fMRI data is how to eliminate the various noise components that are unrelated to the activation but might obscure the results of the statistical analysis. Some of the noise may be attributed to biological sources, such as heartbeat, pulsation of blood vessels, or breathing, that are aliased due to the low scanning rate of 0.5 Hz. It should be noted that high frequency noise aliasing that may be produced by breathing or blood pulsation cannot be removed by simple linear filtering.

In order to address the noise problem, we performed principal component analysis (PCA) (Reyment and Joreskog, 1993) on the entire data set prior to data analysis. This procedure is particularly useful for removing spatiotemporally correlated noise artifacts. The advantage of using PCA is that the filtering is optimized to the data and makes no prior assumptions. The main principal components (PCs) that were filtered were associated with the drift of the magnetic field, correlated breathing fluctuations, and subvoxel motion. Typically, the first two components were removed (see example in Figure 7). The first component depicted a linear temporal drift (this component was apparent also on a phantom scan; therefore, we attribute this component to an external source), and the second component contained high temporal frequency noise that was spatially distributed in a homogeneous manner within the slice. The criterion for removing a component was that it was both spatially not constrained to cortical regions and temporally uncorrelated with the timing of

stimulus presentation. The details of PCA applied to fMRI data are given in the Appendix.

Statistical Tests

Subsequent to the preprocessing stage, the data were analyzed using voxel-by-voxel regression analysis (Friston et al., 1995) to an ideal paradigm. Prior to running the regression analysis, the baseline of each voxel was corrected by removing from each epoch the mean value of the adjacent blank epochs, and each time course of each voxel was linearly transformed into a stochastic process with zero mean and unit standard deviation. This normalization preserved the shape of the time course, but eliminated differences in the absolute amplitudes of the voxels. This process did not change the signal-to-noise ratio, because the linear transformation was applied both to the signal and to the noise.

Pseudo-color maps normalized to match the range of the significant correlation values were generated for each subject and each test. Time courses were derived from clusters of statistically significant voxels, in which the correlation coefficient ranged between 0.4–0.9. The clusters were determined on correlation maps that were spatially smoothed with a 3×3 pixel Gaussian filter, with variance of 1 pixel. The statistical significance of the correlation coefficients was verified by a bootstrap method (Efron and Tibshirani, 1993). In order to derive the statistical significance corresponding to these correlation values, a t-statistic was computed for all voxels and each regression factor:

$$\mathbf{t} = \frac{\hat{\rho} - \rho_{null}}{\hat{\sigma}},$$

where $\hat{\rho}$ is the calculated correlation coefficient, and ρ_{null} is the estimated correlation coefficient of the null hypothesis, i.e., that the time course was uncorrelated to the regression factor (this value was estimated via the bootstrap method).

$$\hat{\sigma}^2 = \sum_{i=1}^{n} (x_i - \hat{\rho} g_i)^2 / (n - 1),$$

where x is the time course of a voxel, g is the regression factor, and n is the number of time points in the factor. Thus, P (the significance level) is: 1-probability (a t-distribution with $n - 1$ degrees of freedom will attain value t). The values given in the figure legends correspond to the estimated P values.

Activation Ratios

In order to compare the strength of activation in two conditions of the same experiment, we calculated activation ratios of these conditions. We define "activation" as mean (activation in condition) minus baseline, where the baseline activation was calculated as the mean value of the minimal activation in each of the blank epochs.

Appendix

Preprocessing fMRI Data Using PCA

In order to enhance the signal-to-noise ratio (SNR) of the data, we performed principal component analysis PCA (Reyment and Joreskog, 1993) on the entire data set prior to data analysis. The mathematics are given below. The SNR of different subjects varied considerably and depended both on external and internal sources; therefore, the number of components that were removed prior to data analysis was not constant. The criterion for the removal of a component was that it was both spatially not constrained to cortical regions and temporally uncorrelated to the timing of stimulus presentation. In order to give a quantitation of the improvement of the SNR by PCA preprocessing, we performed a Kolmogorov-Smirnov (K-S) test aimed at detecting visual active voxels before and after PCA. The SNR was defined as the mean (visual signal) minus mean (blank) divided by the mean standard deviation in the blank epochs. We calculated the SNR in the 20 most significant visual voxels prior to PCA, and then repeated the calculation on the same voxels subsequent to PCA. The SNR improved by a factor of 1.52 ± 0.54 (SD) (in 1 subject it did not improve). Comparing the number of voxels that exceeded a significance of $1e - 4$ showed that before PCA 473 ± 180 voxels exceeded this threshold, and after PCA 1524 ± 600 voxels exceeded this threshold. Thus, on the average the improvement of detectable visual voxels was by a factor of 3.47 ± 1.67 (SD).

Notation

In the following section, matrices will be denoted by bold capital letters and vectors by bold letters. $\mathbf{Y}'$ denotes the transpose of $\mathbf{Y}$, and $\mathbf{Y}^{-1}$ denotes the inverse matrix. $\mathbf{1}_p$ denotes a row vector composed of p ones.

Algorithm

1. Concatenate the data into a matrix $\mathbf{X}$, such that the jth row contains the time course of the jth voxel. The size of this matrix is $N \times p$, where p is the length of the time course and $N = m \times n$ ($[m, n]$ denote the dimensions of the image of the slice). The selected region of interest is sub-matrix $\mathbf{X}_1 \subset \mathbf{X}$ of size $M \times p$ ($M < N$).
2. Normalize all time courses of $\mathbf{X}_1$ by subtracting from each time course its mean value μ_j and dividing the result by its norm. Let $\mathbf{x}_j$ be the jth row of $\mathbf{X}_1$; then, the corresponding normalized time course $\mathbf{y}_j$ is:

$$\mathbf{y}_j = \frac{(\mathbf{x}_j - \boldsymbol{\mu}_j \mathbf{1}_p)}{\sqrt{\mathbf{y}_j \mathbf{y}'}}$$

The normalized matrix $\mathbf{Y}$ is therefore composed of rows of $\mathbf{y}_j$, $j = 1 \ldots M$.
3. Calculate the mean normalized time course:

$$\bar{\mathbf{y}} = \mathbf{1}'_N \mathbf{Y} / \mathbf{1}_N \mathbf{1}'_N$$

4. Subtract the mean normalized time course from $\mathbf{Y}$. Note that after this procedure, both the column and row mean values are zero:

$$\hat{\mathbf{Y}} = \mathbf{Y} - \mathbf{1}'_N \bar{\mathbf{y}}$$

5. Calculate the covariance matrix:

$$Cov\hat{\mathbf{Y}} = \frac{\hat{\mathbf{Y}}' \hat{\mathbf{Y}}}{\boldsymbol{M} - \mathbf{1}}$$

6. Calculate the singular value decomposition of

$$Cov\hat{\mathbf{Y}} = \mathbf{U}' \boldsymbol{\Gamma}^2 \mathbf{U},$$

where $\mathbf{U}$ is an orthonormal matrix of size $p \times p$, and Γ^2 is a diagonal matrix of eigenvalues in descending order of magnitude.
a. Let the eigenvectors matrix $\mathbf{A}$ be: $\mathbf{A} = \mathbf{U}\boldsymbol{\Gamma}$, where each column of $\mathbf{A}$ is an eigenvector.
b. Let the scores matrix $\mathbf{F}$ be: $\mathbf{F} = \mathbf{X}\mathbf{U}\boldsymbol{\Gamma}$.
7. Depict the first eigenvectors (principal components) of $\mathbf{A}$: $\mathbf{A}_1 \ldots \mathbf{A}_j$ (see Figure 1, right), where $\mathbf{A}_j$ denotes the jth column of $\mathbf{A}$, and their corresponding scores $\mathbf{F}_1 \ldots \mathbf{F}_k$, as illustrated in Figure 1 (left).
8. Remove the kth component from the data, by demand from the user, using the following formula:

$$\tilde{\mathbf{X}} = \mathbf{X} - \mathbf{F}_k \mathbf{A}'_k$$

Acknowledgments

This study was funded by ISF grant 131/97. We thank P. Harvey for his crucial contribution to the development of the EPI system, Y. Moses for discussions, and E. Okon for constructing the optical system.

Received January 19, 1998; revised May 28, 1998.

References

Courtney, S.M., and Ungerleider, L.G. (1997). What fMRI has taught us about human vision. Curr. Opin. Neurobiol. *7*, 554–561.

DeYoe, E.A., Felleman, D.J., Van Essen, D.C., and McClendon, E. (1994). Multiple processing streams in occipitotemporal visual cortex. Nature *371*, 151–154.

DeYoe, E., Carman, G., Bandettini, P.A., Glickman, S., Wieser, J., Cox, R., and Neitz, J. (1996). Mapping striate and extrastriate visual areas in human cerebral cortex. Proc. Natl. Acad. Sci. USA *93*, 2382–2386.

Dupont, P., Orban, G.A., De Bruyn, B., Verbruggen, A., and Mortelmans, L. (1994). Many areas in the human brain respond to visual motion. J. Neurophysiol. *72*, 1420–1424.

Dupont, P., De Bruyn, B., Vandenberghe, R., Rosier, A.M., Michiels, J., Marchal, G., Mortelmans, L., and Orban, G.A. (1997). The kinetic occipital region in human visual cortex. Cereb. Cortex *7*, 283–292.

Efron, B., and Tibshirani, R. (1993). An Introduction to the Bootstrap (London: Chapman and Hall).

Felleman, D.J., and Van Essen, D.C. (1991). Distributed hierarchical processing in the primate cerebral cortex. Cereb. Cortex *1*, 1–47.

Ffytche, D.H., Skidmore, B.D., and Zeki, S. (1995). Motion-from-hue activates area V5 of human visual cortex. Proc. R. Soc. Lond. B Biol. Sci. *260*, 353–358.

Friston, J., Homes, A., Worsley, K., Poline, J., Frith, C., and Frackwowiak, R. (1995). Statistical parametric maps in functional imaging: a general linear approach. Hum. Brain Mapping *2*, 189–210.

Goodale, M.A., Meenan, J.P., Bulthoff, H.H., Nicolle, D.A., Murphy, K.J., and Racicot, C.I. (1994). Separate neural pathways for the visual analysis of object shape in perception and prehension. Curr. Biol. *4*, 604–610.

Grill-Spector, K., Kushnir, T., Hendler, T., Edelman, S., Itzchak, Y., and Malach, R. (1998). A sequence of object processing stages revealed by fMRI in the human occipital lobe. Hum. Brain Mapping *6*, in press.

Gulyas, B., Heywood, C.A., Popplewell, D.A., Roland, P.E., and Cowey, A. (1994). Visual form discrimination from color or motion cues: functional anatomy by positron emission tomography. Proc. Natl Acad. Sci. USA *91*, 9965–9969.

Haxby, J.V., Ungerleider, L.G., Horwitz, B., Maisog, J.M., Rapoport, S.I., and Grady, C.L. (1996). Face encoding and recognition in the human brain. Proc. Natl. Acad. Sci. USA *93*, 922–927.

Hirsch, J., DeLaPaz, R.L., Relkin, N.R., Victor, J., Kim, K., Li, T., Borden, P., Rubin, N., and Shapley, R. (1995). Illusory contours activate specific regions in human visual cortex: evidence from functional magnetic resonance imaging. Proc. Natl. Acad. Sci. USA *92*, 6469–6473.

Kanwisher, N., McDermott, J., and Chun, M.M. (1997a). The fusiform face area: a module in human extrastriate cortex specialized for face perception. J. Neurosci. *17*, 4302–4311.

Kanwisher, N., Woods, R.P., Iacoboni, M., and Mazziota, J.C. (1997b). A locus in human extrastriate cortex for visual shape analysis. J. Cogn. Neurosci. *9*, 133–142.

Livingstone, M., and Hubel, D. (1988). Segregation of form, color, movement and depth: anatomy, physiology and perception. Science *240*, 740–749.

Logothetis, N.K., and Sheinberg, D.L. (1996). Visual object recognition. Annu. Rev. Neurosci. *19*, 577–621.

Malach, R., Reppas, J.B., Benson, R., Kwong, K.K., Jiang, H., Kennedy, W.A., Ledden, P.J., Brady, T.J., Rosen, B.R., and Tootell, R.B.H. (1995). Object-related activity revealed by functional magnetic resonance imaging in human occipital cortex. Proc. Natl. Acad. Sci. USA *92*, 8135–8139.

Martin, A., Wiggs, C.L., Ungerleider, L.G., and Haxby, J.V. (1996). Neural correlates of category-specific knowledge. Nature *379*, 649–652.

Orban, G.A., Dupont, P., De Bruyn, B., Vogels, R., Vandenberghe, R., and Mortelmans, L. (1995). A motion area in human visual cortex. Proc. Natl. Acad. Sci. USA *92*, 993–997.

Puce, A., Allison, T., Asgaei, M., Gore, J.C., and McCarthy, G. (1996). Differential sensitivity of human visual cortex to faces, letterstrings and textures: a functional magnetic resonance imaging study. J. Neurosci. *16*, 5205–5215.

Reppas, J., Niyogi, S., Dale, A.M., Sereno, M., and Tootell, R.B.H. (1997). Representation of motion boundaries in retinotopic human visual areas. Nature *388*, 175–179.

Reyment, R., and Joreskog, K. (1993). Applied Factor Analysis in the Natural Sciences (Cambridge: Cambridge University Press).

Salin, P.A., Bullier, J., and Kennedy, H. (1989). Convergence and divergence in the afferent projections to cat area 17. J. Comp. Neurol. *283*, 486–512.

Sary, G., Vogels, R., and Orban, G.A. (1993). Cue-invariant shape selectivity of macaque inferior temporal neurons. Science *260*, 995–997.

Sereno, M.I., Dale, A.M., Reppas, J.B., Kwong, K.K., Belliveau, J.W., Brady, T.J., Rosen, B.R., and Tootell, R.B. (1995). Borders of multiple visual areas in humans revealed by functional magnetic resonance imaging. Science *268*, 889–893.

Talairach, J., and Tournoux, P. (1988). Co-Planar Stereotaxic Atlas of the Human Brain (New York: Thieme Medical Publishers).

Tanaka, K. (1996). Inferotemporal cortex and object vision. Annu. Rev. Neurosci. *19*, 109–139.

Tanaka, K. (1997). Mechanisms of visual object recognition: monkey and human studies. Curr. Opin. Neurobiol. *7*, 523–529.

Tootell, R.B., and Taylor, J.B. (1995). Anatomical evidence for MT and additional cortical visual areas in humans. Cereb. Cortex *5*, 39–55.

Tootell, R.B., Reppas, J.B., Kwong, K.K., Malach, R., Born, R.T., Brady, T.J., Rosen, B.R., and Belliveau, J.W. (1995). Functional analysis of human MT and related visual cortical areas using magnetic resonance imaging. J. Neurosci. *15*, 3215–3230.

Tootell, R.B., Dale, A.M., Sereno, M.I., Malach, R. (1996). New images from human visual cortex. Trends Neurosci. *19*, 481–489.

Tootell, R.B.H., Mendola, J., Hadjikhani, N., Ledden, P., Liu, A., Reppas, J., Sereno, M., Kwong, K., and Dale, A.M. (1997). Functional analysis of V3a and related visual areas in human visual cortex. J. Neurosci. *71*, 7060–7078.

Ungerleider, L.G., and Haxby, J.V. (1994). "What" and "where" in the human brain. Curr. Opin. Neurobiol. *4*, 157–165.

Van Essen, DC., and Drury, H. (1997). Structural and functional analyses of human cerebral cortex using a surface based atlas. J. Neurosci. *17*, 7079–7102.

Young, M. (1992). Objective analysis of the topological organization of the primate cortical visual system. Nature *358*, 152–155.